

OPTIMAL ACTIVE TWIST INPUT SCENARIO FOR ROTOR PERFORMANCE IMPROVEMENT AND VIBRATION REDUCTION

Younghyun You*, Manoj K. Dhadwal*, and Sung N. Jung*

*Dept. of Aerospace Engineering, Konkuk University, Seoul, South Korea

Abstract

In this paper, the best actuation scenario is sought using a multitude of active twist control inputs taking advantage of a global search algorithm to improve performance and reduce vibration of a helicopter rotor. The active twist schemes include a single harmonic, multiple harmonic, and three other segmented non-harmonic actuation cases. An advanced particle swarm assisted genetic algorithm (PSGA) is employed for the optimizer. In addition, a comprehensive rotorcraft analysis code CAMRAD II is used to reach the trim and to predict the rotor power and hub vibratory loads. A scale-down BO-105 model is used for the reference rotor and the actuator material is assumed to be embedded in the blade structure. The numerical simulation is carried out for low speed descent and high speed forward flight conditions. Among the active twist control inputs, the non-harmonic cases show the best performance gains in reducing the hub vibrations and power consumptions. The hub vibration is reduced by up to 75% while the rotor power is decreased by 2.8% as compared to the baseline uncontrolled rotor at the low speed descending flight condition. The resulting optimized actuation profiles for each of the active twist control cases are found denoted as a function of amplitudes and phases of the rotor response.

1. INTRODUCTION

During the past decades, high vibration and noise, and relatively low performance characteristics mainly due to the rotation of the rotor have been the key issues of concern in rotorcraft aeromechanics field. A variety of active control concepts and mechanisms have been studied as potential applications to tackle the problem. Among the proposed methods, the active twist rotor (ATR) concept offers clear advantages such as the fact that no hydraulic power systems and/or separate mechanical parts are required since the rotor blades are directly twisted by induced-strain actuators embedded in the rotor blade structure. The ATR is pioneered by Chen and Chopra [1] exploiting the benefit of direct strain components of piezoelectric coefficients. The detailed discussion of ATR and its development are found in Chopra [2], Thakkar and Ganguli [3], and Pawar and Jung [4].

The first and the most widely explored ATR technique uses a single harmonic type of control input introduced into the rotor blade individually. The amplitude and phase of a given higher harmonic frequency are varied arbitrarily for the twist control. The representative study under this category is the so called NASA/Army/MIT active twist rotor [5-6] tested in the NASA Langley Transonic Dynamics Tunnel at various flight speeds. Either of 3 to 5/rev actuation is applied to the actuator region resulting in a significant vibration and blade-vortex interaction (BVI) noise reduction. Yeo [7] investigated the capability of the existing active control concepts

including the active twist control. A 2/rev harmonic ATR input is used for the improvement in the rotor performance. The rotor lift-to-drag ratio becomes increased by about 10% at high speed conditions with slight reduction in blade loading. Recently, an international joint program called STAR (Smart Twisting Active Rotor) is formed to benefit the active twist concept for performance improvement, vibration reduction, and noise alleviation of a rotor [8]. Up to 5/rev active twist harmonic inputs are applied for a variety of flight conditions of the rotor and it shows a potential in reaching the desired goals. The first type of control is simple to apply, but the actuation is limited to the specified wave form adopted in the harmonic function.

The next one uses a multi-harmonic twist input that combines a number of higher harmonic components. Strictly speaking, the single harmonic actuation is a subset of the second type. However, they are divided into separately to clearly understand the benefit of the twist control with each other. Zhang et al. [9] and Bailly et al. [10] use a combined input comprised of up to 5/rev harmonics to demonstrate the potential improvement of ATR with respect to rotor performance, vibration and noise reduction. The multi-harmonic type of control offers a broad spectrum of harmonic inputs to enlarge the actuation authority when compared with the single harmonic counterpart, while the complexity become increased significantly due to larger design space in the multiple inputs.

The final one is the non-harmonic type of twist inputs that has been studied recently. In this case, arbitrary

waveforms such as a step or saw-type input are generated to activate the blade. Fogarty et al. [11] uses a step input to examine the BVI noise characteristic according to the actuation of MFC (Macro Fiber Composites) actuator plies embedded in a portion of an Apache AH-64A blade. The step input is characterized by rotor azimuthal location to start, duration, and magnitude of actuation. A promising noise reduction of up to 10 dB in BVI noise is reached with the non-harmonic active control. It is indicated that the noise reduction performance is highly dependent on the initial azimuthal location and the duration of the actuation. Jain et al. [12] investigated several on-blade active controls including the active twist control for improving rotor performance. An advancing-side-only actuation with 2/rev harmonic form is adopted in the twist control. The study reveals that the proposed waveform is efficient in improving the performance of a rotor in high speed flight where the outboard tip region is subjected to a negative loading. These non-harmonic active twist actuation studies show great potential in reducing BVI noise and increasing performance gains. However, only single step or a simple harmonic waveform has been introduced for the actuation. To maximize the actuation performance, there is a need to make use of more general forms of harmonic or non-harmonic waveform shapes suited to the rotorcraft operation environment.

The objective of the current work is to find the best actuation deployment scenario using various types of ATR inputs taking advantage of a global search algorithm for performance improvement and vibration reduction. The actuation scenarios include a harmonic, multiple harmonics, and segmented non-harmonic inputs. An advanced particle swarm assisted genetic algorithm (PSGA) [13] is employed for the optimizer, while the comprehensive rotorcraft analysis code CAMRAD II [14] is used to compute the rotor response. The simulation results are presented in three different sections. First, the optimization algorithm used is verified by conducting an actuation parameter sweep study in terms of actuation magnitudes, excitation frequencies, and phase angles. Next, the rotor performance improvement or vibration reduction is studied in low speed descending flight and high speed forward flight conditions. In addition, the relative performance indices obtained between the actuation scenarios are compared with reference to the baseline uncontrolled case. Finally, a simultaneous vibration reduction and performance improvement of the rotor is sought using a multi-objective function.

2. ANALYSIS METHODS

The analysis methods and optimization algorithms are described in the following sections. The active

twist input schedules are also discussed.

2.1. Optimization algorithm: PSGA

An advanced global search algorithm PSGA [13] is employed for the present study. The PSGA consists of two phases: the particle swarm (PS) and the genetic algorithm (GA) phase. The PS phase regulates the enhancement of worst solutions by using the global-local best inertia weight and acceleration coefficients to increase the overall efficiency. In the GA phase, a rank-based multi-parent crossover (RMPC) is used which is formulated through the modification of crossover and mutation operators leading to concurrent exploration of local and global optimum solutions. The polynomial mutation with a variable mutation probability is used for the genetic diversity. Furthermore, the Euclidean distance-based niching implemented in the replacement phase of GA assists in maintaining the population diversity. To avoid settling in the local optimum solutions, the stagnation check is performed and the solution is randomized in the design space when needed. A feasible population-based relaxation scheme is used to deal with the linear as well as nonlinear constraints. The optimization loop is continued until the global optimum solution is reached or any of the termination criteria are satisfied. Figure 1 shows the overall flow chart of the PSGA optimization algorithm.

The total population size adopted in the present work

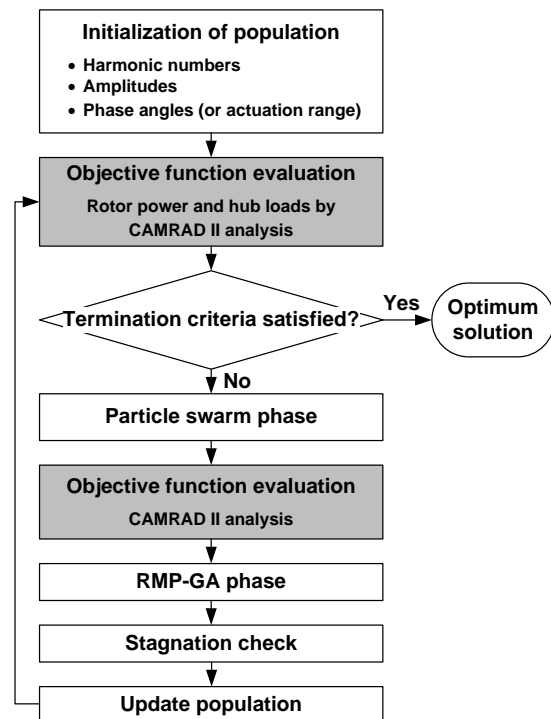


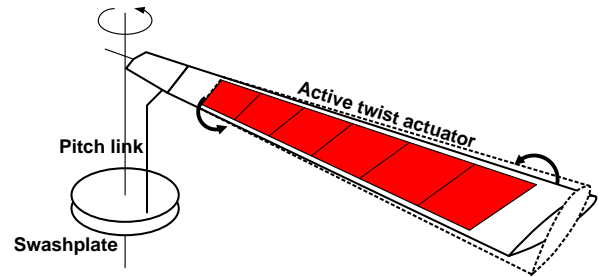
Fig. 1 Flow diagram of PSGA optimization algorithm.

is 20 with 10 each for the PS and GA phases. The binary tournament selection is used as a selection scheme in the GA. For the RMPC operator, the limits of the scaling factor are set to $S_{\min} = 0.5$, $S_{\max} = 0.98$ while the crossover rate are varied between 0.8 and 0.98. Since the parameters are self-adaptive, no tuning is necessary [13].

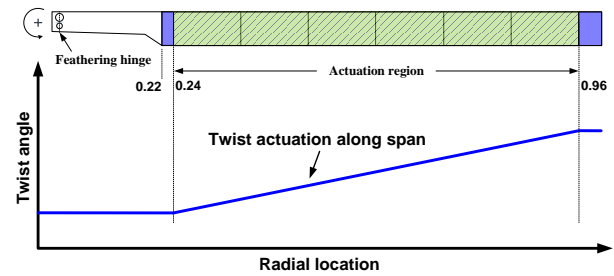
2.2. Comprehensive rotorcraft analysis code: CAMRAD II

A comprehensive rotorcraft dynamics analysis code CAMRAD II [14] is used to analyse the rotor. It is characterized by multibody dynamics, nonlinear finite elements, and various levels of rotorcraft aerodynamic models. For the structural analysis, the blade motion is expressed as the summation of the rigid body motion and the elastic motion. The rigid body motion describes the motion of one end of a beam element, and the elastic motion is measured relative to the rigid body motion. The beam elements are represented by three translational (axial, flap, and lead-lag) and three rotational degrees of freedom (DOF) resulting in a 15 DOF beam element. The aerodynamic model of CAMRAD II is based on a lifting-line theory combined with an airfoil table look-up as well as various levels of the vortex wake representation. In this study, the blade structure is discretized into 18 nonlinear beam finite elements distributed along the blade span length. An ONERA-EDLIN unsteady aerodynamic theory along with C81 airfoil table look-up is used to compute the airloads acting on the blade. In addition, a rolled-up free wake model is used to compute the non-uniform induced inflow around the rotor. The rolled-up wake model is based on the feature that a tip vortex forms at the blade tip. Only an isolated rotor condition is considered to simplify the analysis.

CAMRAD II does not provide an option to allow modelling the induced strain actuation of a piezoelectric actuator. Therefore, the active twist model is implemented through the application of torsional couple with equal and opposite magnitudes at the extremities over the actuation zone of the blade. Figure 2 shows the schematic of the active twist control mechanism of a blade under the action of torsional couple. It is assumed that the MFC actuator is embedded in the skin of the blade structure, spanning from 24% to 96% blade radial stations. The applied torsional couple results in a linear variation of twist angle along the blade span length while no twist variation exists in the free-actuation region. Note that a positive twist moment produces a change in the nose-up pitch angle. The actuator region is modelled with 6 beam finite elements. The effect of the embedded piezoelectric actuator on the blade section properties is ignored.



(a) Active twist control by twist moment couple



(b) Twist angle distribution along radial location

Fig. 2 Active twist control schematic.

2.3. Active twist input scenarios

The twist actuation schedules tuned to specific flight conditions and operation environments of a rotor are crucial to meet the desired goals of achieving the minimum vibration and the maximum performance. A total of five different ATR scenarios are introduced taking into consideration of the complex nature of the rotor aeromechanics and its interaction with other disciplines (e.g., vibration and noise). These include single harmonic, multiple harmonic, and three non-harmonic types of twist control schedules. Figure 3 illustrates the schematic views of each twist control scenarios depicted over the rotor disk and the way active control works distributed along the rotor azimuth angles. The shaded region indicates the zone where the twist actuation is applied whereas the blank region indicates no actuation zone.

The Case 1 is a single harmonic input that has been studied extensively during the previous decades. In this schedule, each blade is actuated harmonically over the whole rotor disk (without pause) with a function as given by

$$(1) \quad T(\psi) = A \cos(n\psi - \phi)$$

where A is the amplitude of twist moment, n is the single harmonic number, and ϕ is the phase angle. The schedule is the most simple and the number of design variables is three for the optimization problem that include the amplitude, phase angle, and actuation frequency.

The next one (Case 2) is a multi-harmonic actuation that combines a few harmonic signals with different

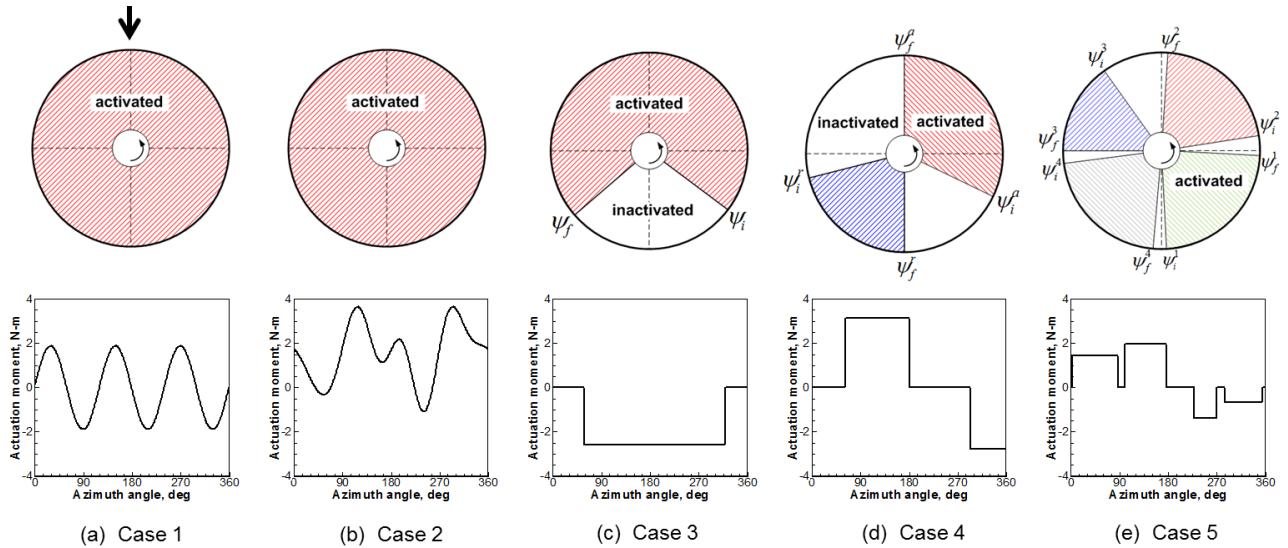


Fig. 3 Actuation input scenarios for active twist control.

frequencies. The frequency contents spanned from 2 to 5/rev (integer multiples of the rotating frequency) are exploited for the study. This leads to nine design variables such as the steady signal, and the amplitudes and phase angles for each of the four actuation frequencies. A general form of the multi-harmonic control law can be given as

$$(2) \quad T(\psi) = B_0 + \sum_{n=2}^5 B_n \cos(n\psi - \phi_n)$$

where B_0 is the steady moment, B_n and ϕ_n are the amplitude and phase of the n -th harmonic frequency.

The other three schedules (Case 3 to 5) are non-harmonic waveform inputs composed based on the step-type functions. The actuator is activated uniformly only for the designated regions. As can be seen from Figs. 3c to 3e, the rotor disk area is split into zones with activation or inactivation according to the cases considered. The shaded regions indicate the application of non-zero twisting moment actuation. The design variables of non-harmonic inputs include the actuation magnitude and rotor azimuthal location to start and duration. In Case 3 (Fig. 3c), the actuation is performed once per revolution over the entire rotor disk. Fogarty et al. [11] adopted this kind of single non-harmonic type input for the reduction of acoustic noise emission of a rotor. The number of design variables is three in this case. For Case 4 (Fig. 3d), either the advancing side or the retreating side of the rotor disk is subjected to separate control with different magnitudes of twist moment. This scenario is more tuned to the aerodynamic environment of a rotor where the advancing side suffers from increased risk of shocks and BVI while the retreating side is under reversed flow and stall. The number of design variables is six since the separated disk area. Jain et

al. [12] explored this type of non-harmonic actuation input to control the trailing-edge flap deployment for improved performance. The last Case 5 scenario considers each quadrant of the rotor disk separately as depicted in Fig. 3e. This case is particularly suited to deal with BVI related phenomena. In general, the interacting vortices are generated in the second and third quadrants while the BVI events are placed in the first and fourth quadrants referenced from the rear of the disk. The number of design variables is twelve due to the separation of the rotor disk by four quadrant regions. It should be noted that this type of non-harmonic actuation along with Case 4 has never been attempted for active twist control of a rotor.

The non-harmonic input is suggested using arbitrary function shapes, however, the blade response is harmonic in nature. CAMRAD II also accepts the harmonic components as input parameters. The Fourier analysis is carried out to compute the harmonic components of the given (non-harmonic) step function which are combined to produce an equivalent harmonic type input to be used in CAMRAD II. Harmonics of 0-19/rev components are combined to represent the step function for the present study. Figure 4 presents a non-uniform step-type function and its transformed input by harmonic combinations with 0-19/rev. The abrupt changes of the signal become smoothed around the corners, while the constant magnitude is replaced with oscillatory signals after the operation of the Fourier analysis. The difference is expected to be negligible for blade responses.

The general non-harmonic control law for the cases with non-uniform actuation can then be given by

$$(3) \quad T(\psi) = B_0 + \sum_{n=1}^{19} B_n \cos(n\psi - \phi_n)$$

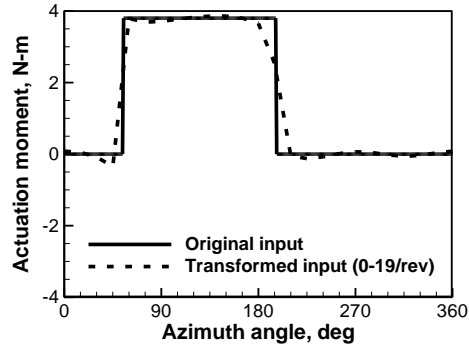


Fig. 4 Non-harmonic input for CAMRAD II input

The amplitudes of the twist moment, starting and ending azimuths (ψ_i and ψ_f) all constitute the design variables for each case of the three non-harmonic scenarios.

2.4. Optimization framework

In this study, a multi-objective optimization problem is set to minimize the hub vibratory loads and rotor power required, either by individually or collectively. The arbitrary weight factors are introduced to control the relative contribution of the constituent objective functions, which is stated as:

Minimize:

$$(4) \quad f(\mathbf{x}) = w_1 \frac{P(\mathbf{x}) - P_0}{P_0} + w_2 \frac{VI(\mathbf{x}) - VI_0}{VI_0}$$

with bounds for design variables as:

$$(5) \quad \mathbf{x}^L \leq \mathbf{x} \leq \mathbf{x}^U$$

where w_1 , w_2 are the weight factors, \mathbf{x} is the design variables vector with \mathbf{x}^L and \mathbf{x}^U as the lower and upper bounds, respectively, and subscript '0' indicates the baseline values. $P(\mathbf{x})$ and $VI(\mathbf{x})$ represent the total power required and the vibration index, respectively. The vibration index (VI) is determined from the 4/rev and 8/rev hub force and moment components (4-bladed case) and is defined in a form as [8, 15]:

$$(6) \quad VI = \sum_{i=4,8/\text{rev}} \left[\frac{\sqrt{(F_{x,i}/2)^2 + (F_{y,i}/1.5)^2 + F_{z,i}^2}}{W_0} + \frac{\sqrt{M_{x,i}^2 + M_{y,i}^2}}{W_0 R} \right]$$

where $F_{x,i}$, $F_{y,i}$, $F_{z,i}$ represent the hub shear forces, and $M_{x,i}$, $M_{y,i}$ represent hub moments with x , y , z denoting longitudinal, lateral, and vertical directions, respectively. The subscript i indicates the 4/rev or 8/rev hub vibratory components. W_0 is the reference weight of a rotorcraft and R is the rotor radius.

An optimization framework is developed to find the optimum active twist control inputs. It has been built

around an evolutionary algorithm PSGA, which has been coupled with CAMRAD II. Figure 1 shows the overall flowchart of the present optimization framework. The procedure for optimal active twist input using PSGA is described as: The reference points for the rotor power required, vibration, and noise are calculated first. Next, a CAMRAD II input file is constructed and provided as an input for the optimizer. The input file contains the harmonic values with respect to the active twist input. The optimization algorithm PSGA then generates the initial candidate solutions in the specified design search space. The suggested input data are again fed into CAMRAD II for the computation of rotor power and hub vibratory loads. The resulting outputs are used to evaluate the objective function. The updated design solutions are ranked according to the feasibility represented by the computed objective function values. The optimization loop is continued until the optimum solution is reached.

3. RESULTS AND DISCUSSION

The HART (Higher harmonic Aeroacoustic Rotor Test) II rotor tested at the German-Dutch wind tunnel (DNW) in 2001 [16] is used as the reference rotor. The rotor has a four-bladed hingeless configuration with a solidity 0.077 and blade radius 2 m. The HART II rotor installed with MFC actuators under the skin structure is considered as ATR which is designated as HART II ATR. Figure 5 shows the elastic twist response at the blade tip of the rotor in hovering flight condition with respect to the increase in the actuation moment. The twisting couple is varied up to 4 N-m by an interval of 1 N-m. As can be seen, a pure linear behaviour is obtained with the application of the twist moment couple.

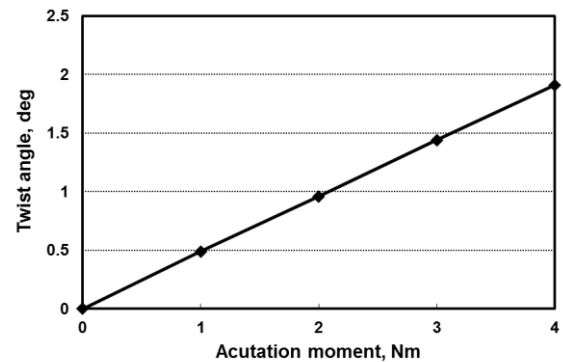


Fig. 5 Blade tip elastic twist angle versus applied actuation couple in hover.

In the following sub-sections, results using the proposed optimization framework are validated considering Case 1 against those by the conventional parameter sweep study. Then the improvements in vibration and performance of HART II ATR in descending ($\mu = 0.15$) and high speed flight

($\mu = 0.34$) are examined for different actuation schedules employed in the present study.

3.1. Rotor trim

The rotor trim is investigated first. In the wind tunnel test of HART II rotor, a zero-moment trim is set to match the trim targets. This trim strategy is acceptable for vibration and noise prediction study, however, lacks reliable estimation of the performance (e.g., power required) since the propulsive force or drag is not taken into account in the trim [17]. A propulsive trim method is preferred to identify the pure effect of active twist input on the performance improvement. For the propulsive trim, the rotor drag force is calculated using the follow equation [18].

$$(7) H_x = \rho \pi R^4 \Omega^2 \frac{\sigma c_{d0}}{8} (3\mu + 1.98\mu^{2.7})$$

where ρ is the air density and Ω is the rotating speed. σ represents solidity, c_{d0} represents mean airfoil drag coefficient, and μ represents advance ratio. Table 1 shows the trim targets set between HART II and HART II ATR in descent condition.

Table 1. Comparison of trim targets in descent flight condition.

HART II		HART II ATR	
Thrust, N	3300	Thrust, N	3300
Hub roll, Nm	-20	Drag force, N	24.6
Hub pitch, N-m	-20	Hub roll, N-m	0

The influence of trim target changes on trim control values are investigated for HART II baseline (BL) condition. Figure 6 shows the comparison of trim control angles between the measured data [16], predicted HART II results [19], and the present predictions on HART II ATR. The predicted results of HART II ATR are in good correlation with the earlier HART II results whereas the correlation is satisfactory when the comparison is made with the measured values. The reason of discrepancy in the lateral cyclic angle θ_{lc} is associated with the neglect of the fuselage model in both analytical predictions [20]. Figure 7 shows the predicted tip elastic twist and torsion moments of HART II ATR as compared with those of HART II. It is observed that no significant variation of the blade motion is obtained with the trim target changes. These results indicate that the newly configured trim target is acceptable to study further with HART II ATR.

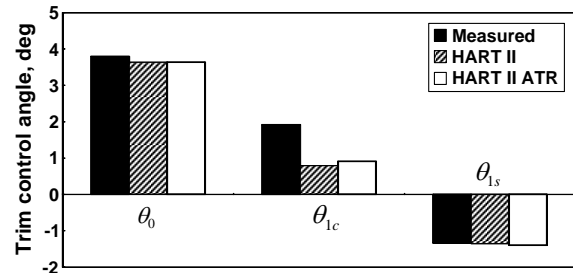
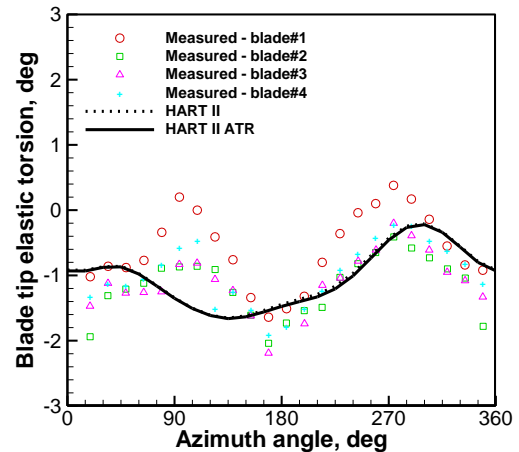
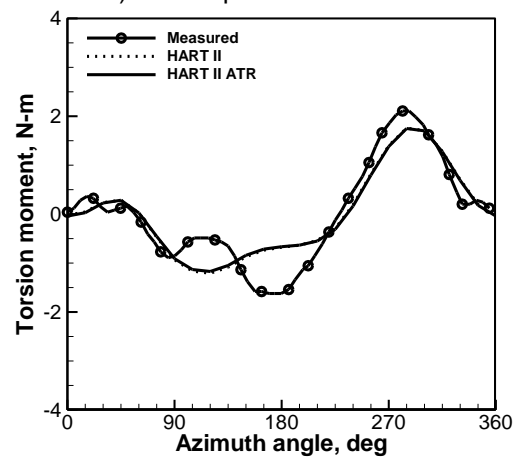


Fig. 6 Comparison of trim control angles by trim target change.



a) Blade tip elastic torsion



(b) Torsion moment (0.33R)

Fig. 7 Comparison of tip elastic twist and torsion moments with respect to trim target changes.

Using the propulsive trim setup, the validation of optimum results and the effect of active twist control on rotor performance improvement and vibration reduction is evaluated for low speed descending ($\mu = 0.15$) and high speed forward flight ($\mu = 0.34$) conditions in the next sections.

3.2. Validation of optimum result

The parametric sweep study at the single harmonic

input condition (Case 1) is carried out to identify the behaviour of vibration and performance with respect to the amplitude and phase angle sweep and to validate the optimum results. To this end, the amplitude of twist couple is varied from 1 to 4 N-m with 1 N-m intervals and the phase angle is swept from 0° to 360° with 60° for the respective actuation frequencies at 2 to 5/rev. Either descending or high speed forward flight condition is used for the study.

Figure 8 shows the percentage change in the total power required with reference to the baseline (no actuation) at the descent flight condition ($\mu = 0.15$). It is observed that the higher amplitude input increases the rotor power required. A 2/rev actuation with 1 N-m amplitude at 300° phase angle appears the most effective in reduction of total power required. Similar results are observed at high-speed condition though not presented explicitly.

Figure 9 shows the variation of vibration index from baseline condition due to parameter sweep study at the high-speed forward flight condition ($\mu = 0.34$). The most effective actuation frequency for reducing vibration is 3/rev in high speed flight. The minimum vibration seems to be achieved with 1 N-m amplitude at 180° phase. It is noted that, with 4/rev input, the vibration increased greatly compared with the baseline condition.

At the 3/rev actuation frequency, the sine and cosine component of the 4/rev hub vibratory forces and moments are plotted in Fig. 10. The center of each circle represents the baseline value. All hub vibratory loads show counter-clockwise variation due to the phase sweep. It is seen from the figures that the larger amplitudes generate larger variations in the vibratory hub loads. The minimum hub shear forces are possible between 1 N-m and 2 N-m amplitudes. The maximum reduction in hub rolling moment is observed between 3 N-m to 4 N-m amplitudes. The minimum hub pitching moment is achieved at near 2 N-m amplitude with 120° phase angle. In particular, it is observed that the phase angles for minimum vibration at all vibration components are between 120° and 180° .

The optimum single harmonic input for performance improvement or vibration reduction is found using the present optimization framework. The resulting optimum values are correlated then with those by the parametric sweep study performed above. Table 2 shows the comparison between the sweep results and the optimum solutions computed using PSGA obtained for the rotor power required at both flight conditions. A reliable correlation appears reached for the two different sets of predictions. Note that the optimization is employed with much finer resolutions ($\Delta A = 0.1$ Nm, $\Delta \phi = 1^\circ$) as compared to the sweep study ($\Delta A = 1$ Nm, $\Delta \phi = 60^\circ$) leading to slightly

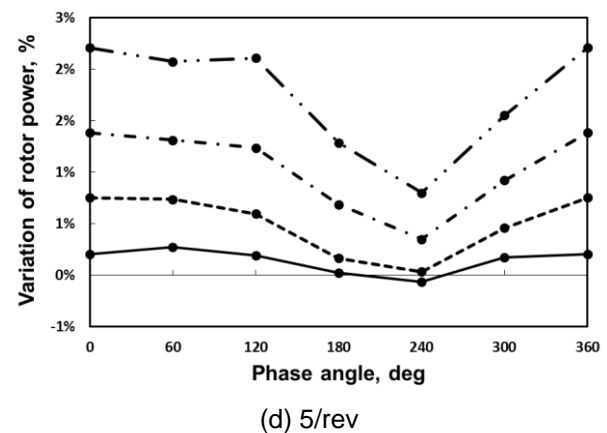
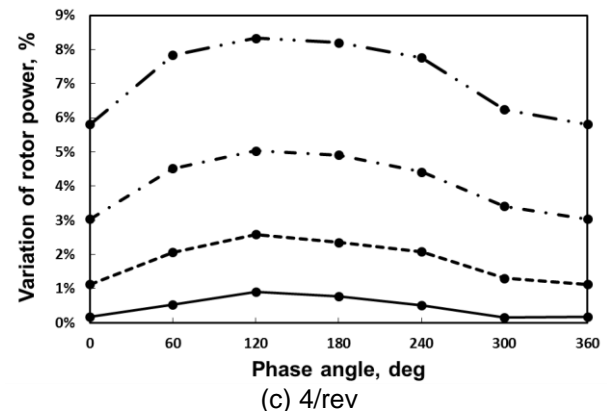
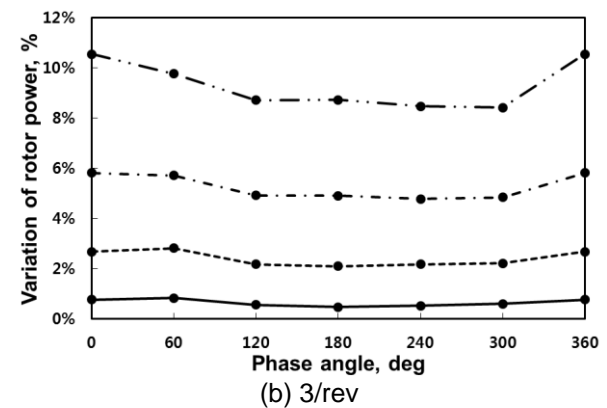
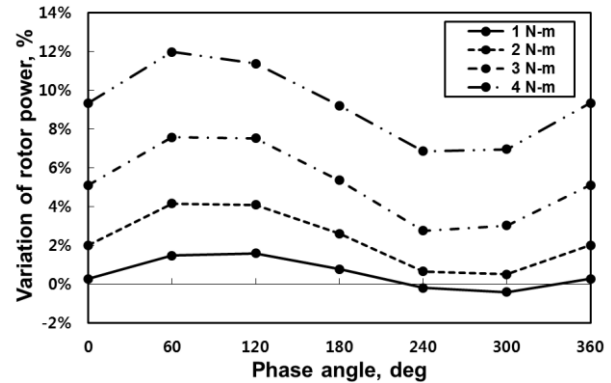


Fig. 8 Variation of total power required due to amplitude/phase sweep ($\mu = 0.15$).

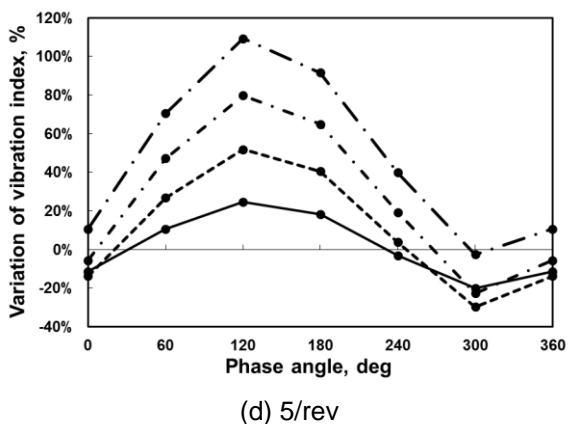
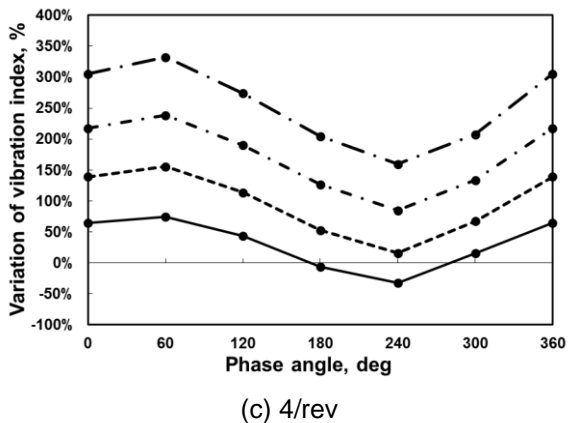
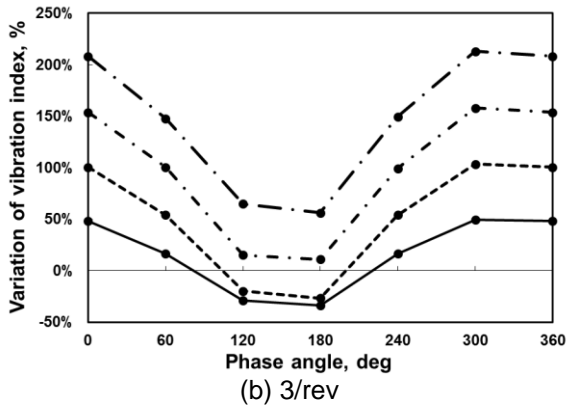
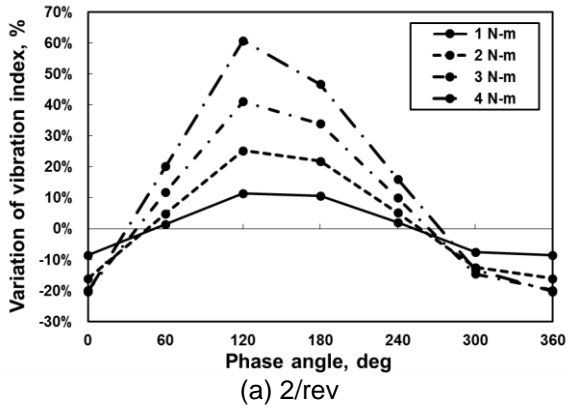


Fig. 9 Variation of vibration index due to amplitude/phase sweep ($\mu = 0.34$).

Table 2. Comparison of optimum single harmonic input for minimum power required.

	Descent		High speed	
	Sweep	Optim um	Sweep	Optim um
Amplitude (Nm)	1	0.8	3	1.6
Harmonic number	2/rev	2/rev	2/rev	2/rev
Phase angle	300°	276°	240°	254°
Variation	-0.40%	-0.45%	-0.65%	-0.68%

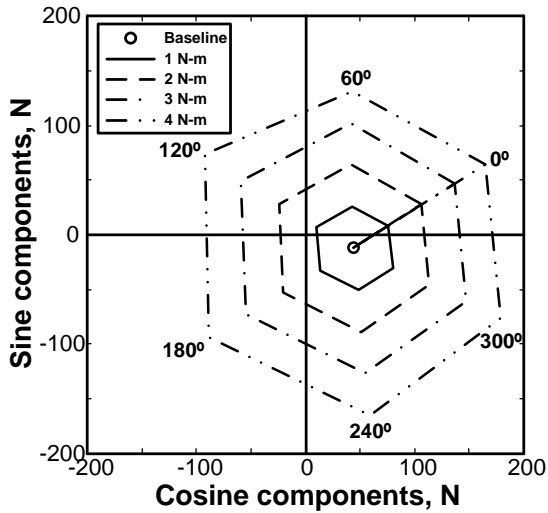
Table 3. Comparison of optimum single harmonic input for minimum vibration.

	Descent		High speed	
	Sweep	Optim um	Sweep	Optim um
Amplitude (Nm)	2	1.9	1	1.5
Harmonic number	3/rev	3/rev	3/rev	3/rev
Phase angle	180°	175°	180°	154°
Variation	-49%	-52%	-32%	-52%

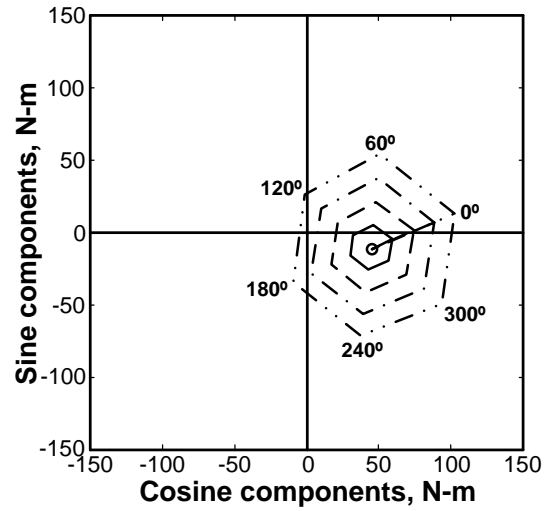
improved gains in vibration and performance perspectives. Table 3 shows the comparison of optimum results against those of the sweep study for the vibration index. The optimum input for performance and vibration is predicted reasonable since the phase angles obtained are similar to the results of the parametric study. In addition, the optimum algorithm leads to increased gains up to 20% due to the use of finer search space interval of design variables. Based on the comparison results, it is believed that the optimum algorithm is suited for finding the best active twist control schedules at given flight regimes.

3.3. Optimum result at descent flight condition ($\mu = 0.15$)

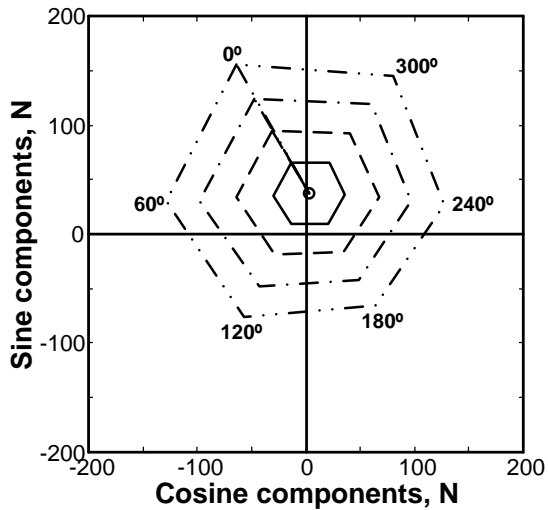
The simulation results for the optimal actuation scenarios of the rotor in descending flight are discussed in this section. Figure 11 shows the percentage reduction in the power required and the overall vibration index obtained for the five different cases with respect to the baseline uncontrolled rotor



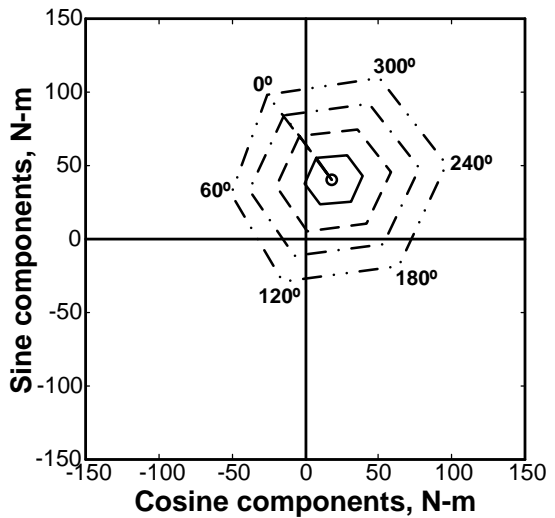
(a) Longitudinal hub shear force



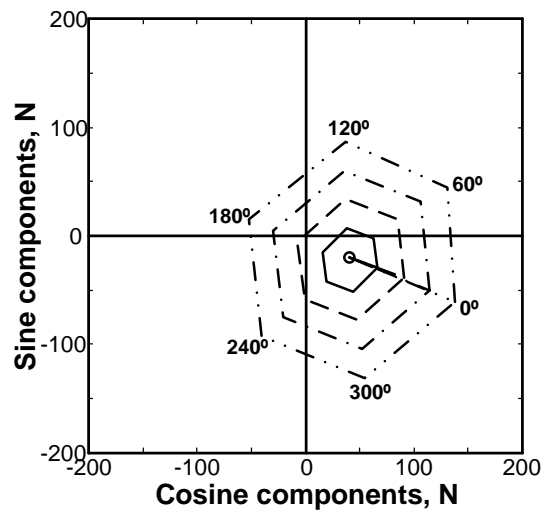
(d) Hub rolling moment



(b) Lateral hub shear force



(e) Hub pitching moment



(c) Vertical hub shear force

Fig. 10 Variation of 4/rev hub vibratory components due to phase sweep in high-speed flight ($\mu = 0.34$).

when the objective function is set to maximize the rotor performance only (see Eq. 4). As can be seen, the non-harmonic twist schedules show better performance gain than the harmonic counterparts. The best performance gain is observed with Case 4, which exhibits a reduction in the total power required by 2.8%, while only 0.45% power reduction is obtained in Case 1. Given the objective function set for the performance, the VI becomes increased for most cases. For Case 3, however, the overall vibration is reduced by about 45%. This result demonstrates that both performance improvement and vibration reduction can be achieved when an appropriate control law is adopted. Figure 12 shows the respective actuation schedules of Case 3 and 4, which show remarkable gains, as compared with Case 1. A similar trend is seen between the cases,

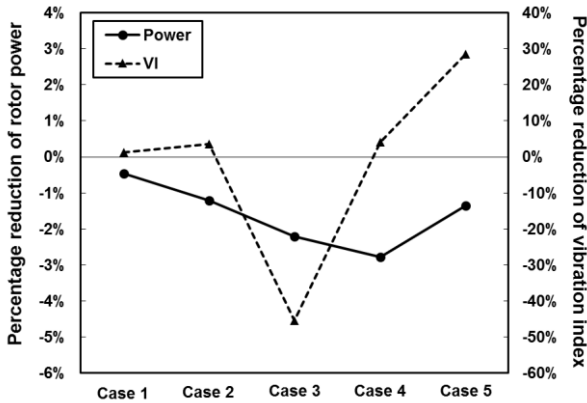


Fig. 11 Percentage reduction of rotor power and vibration at the performance optimum input ($\mu = 0.15$).

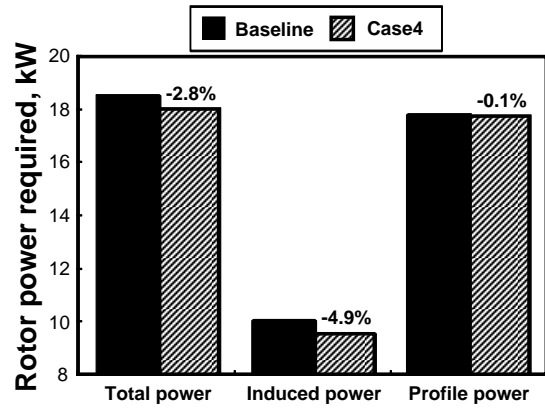


Fig. 14 Composition of rotor power at the minimum power condition of Case 4 ($\mu = 0.15$).

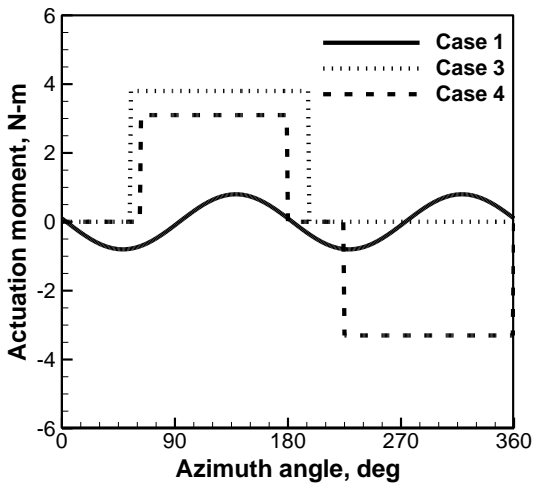


Fig. 12 Optimum input scenarios for performance improvement ($\mu = 0.15$).

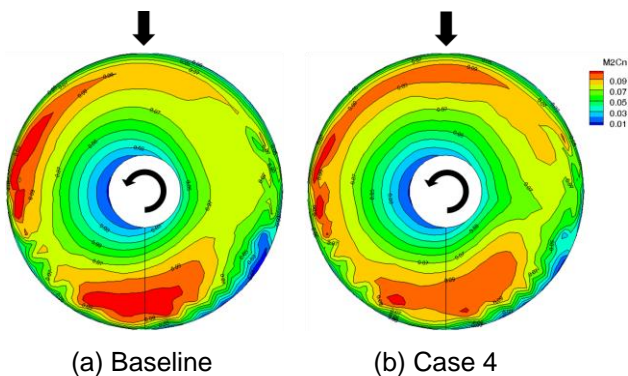


Fig. 13 Comparison of section airloads ($\mu = 0.15$).

particularly in the second quadrant of the advancing side where all the cases are under a pitch-up actuation, whereas the retreating side is under different pitch inputs. The negative twist moment produced in the retreating side of Case 4 contributes

the additional gains in the power required. The physical mechanism leading to the improvement in the performance can be explained using the distribution of section airloads over the rotor disk. Figure 13 shows the section normal force coefficients obtained for ATR with Case 4 as compared with the baseline uncontrolled case, presented in a contour plot. The time step size used for the airloads distribution is 5° . It is observed that, in the minimum power condition (Case 4), the normal force distribution becomes more uniform compared to the baseline condition. The zones with peak values met in the retreating side and the rear region of the baseline rotor are decreased substantially while the lift in the second quadrant of the rotor is increased slightly. It should be noted that the zero roll moment is prescribed while maintaining the thrust level for all the cases considered. More flattened distribution of airloads with Case 4 helps in improving the performance of the rotor. Fig. 14 shows the composition of the power required for the optimum Case 4 that consists of induced power and profile power as compared to the baseline. As seen in the figure, almost all the performance improvement is caused by the induced power reduction. This result is again assisted the observation made with the redistribution of airloads (Fig. 13) due to the active twist input applied to the rotor. So far, the objective function is considered with the performance perspective. The vibration response is investigated next.

Figure 15 shows the percentage reduction in the power required and the overall vibration of the five control scenarios when the objective function is dealt with the rotor vibration only (see Eq. 4). As expected, the vibration levels for all the cases show significant reduction while the required power indicates large variation according to the active twist schedules. Among the active twist inputs, Case 2 exhibits the best vibration reduction with negligible changes in the power required, while Case 4 shows a substantial reduction in both disciplines. In this case,

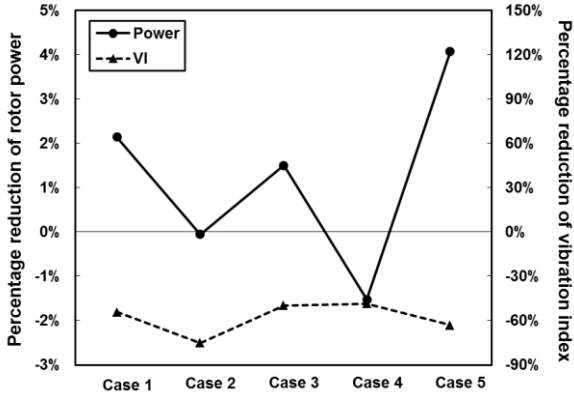


Fig. 15 Percentage reduction of rotor power and vibration at the vibration optimum input ($\mu = 0.15$).

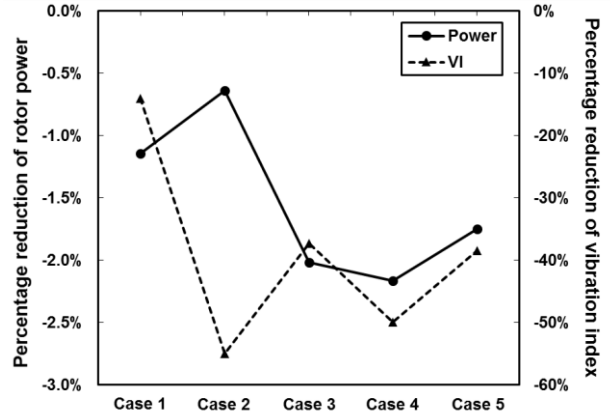


Fig. 18 Percentage reduction of rotor power and vibration with the multi-objective input ($\mu = 0.15$).

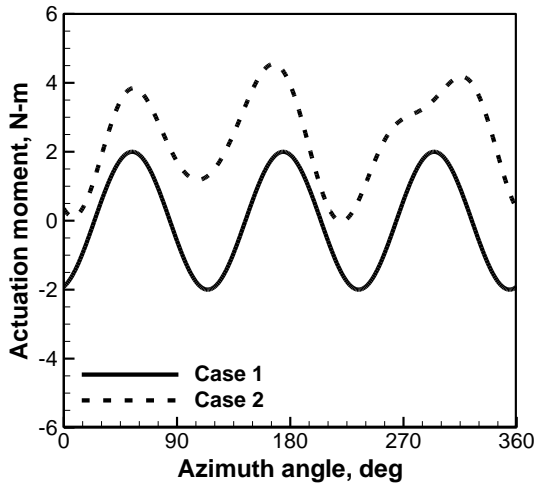


Fig. 16 Optimum input scenarios for vibration reduction ($\mu = 0.15$).

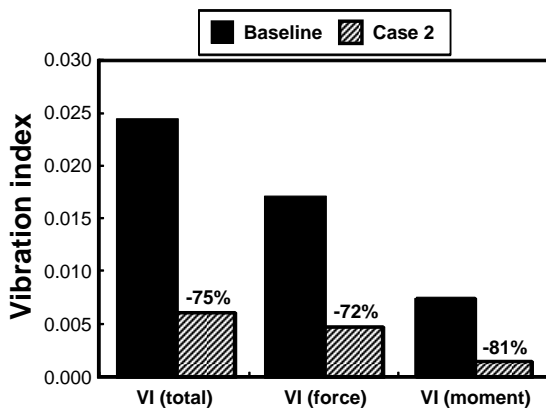


Fig. 17 Composition of vibration at the minimum vibration condition of Case 2 ($\mu = 0.15$).

the reduction is about 48% for the vibration index and 1.5% for the power required. In Figure 16, the best active twist schedule (Case 2) obtained for the vibration is compared with that of Case 1. The two cases show similar wave forms but with apparent offsets. The Case 2 input produces positive (pitch-up direction) twist moment when compared with Case 1. Figure 17 shows the composition of the vibration index for Case 2. Both the shear forces and moment components become decreased collectively leading to a reduction of about 75% based on the uncontrolled rotor.

A simultaneous reduction of the power required and the overall vibration is attempted using the multi-objective function (Eq. 4). Since the performance and vibration parameters in the multi-objective function are fundamentally different with each other, an appropriate scaling is necessary to make the order of magnitudes between the two nearly equal. In this study, the weight factor at the performance parameter for each of the five scenarios is varied to match the corresponding vibration measure. Figure 18 shows the percentage reduction of power required and vibration with respect to the baseline values. With the multi-objective optimization, the total power and the overall vibration are decreased simultaneously for all the actuation cases considered. The results indicate that Case 4 has significant potential for vibration reduction and performance improvement. The vibration index is reduced by 50% and the power required is decreased by 2.2%. It is noted that the weight factors can be varied accordingly to obtain desired optimum gains for vibration or performance.

3.4. Optimum result at high-speed forward condition ($\mu = 0.34$)

Next, the best actuation scenario is sought for the rotor in high speed forward flight. Figure 19 shows the percentage reduction in the rotor power required

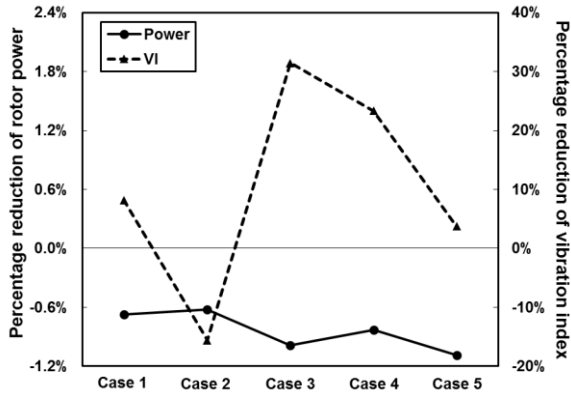


Fig. 19 Percentage reduction of rotor power and vibration at the performance optimum input ($\mu = 0.34$).

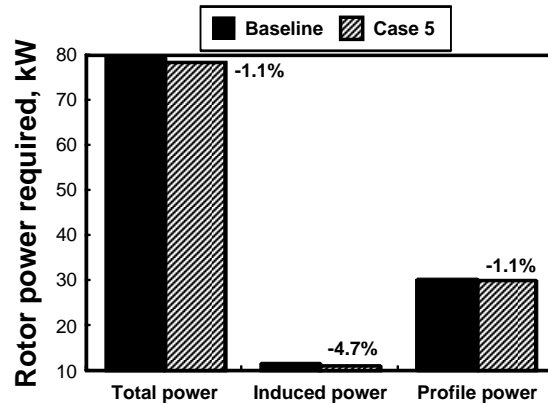


Fig. 22 Composition of rotor power at the minimum power condition of Case 5 ($\mu = 0.34$).

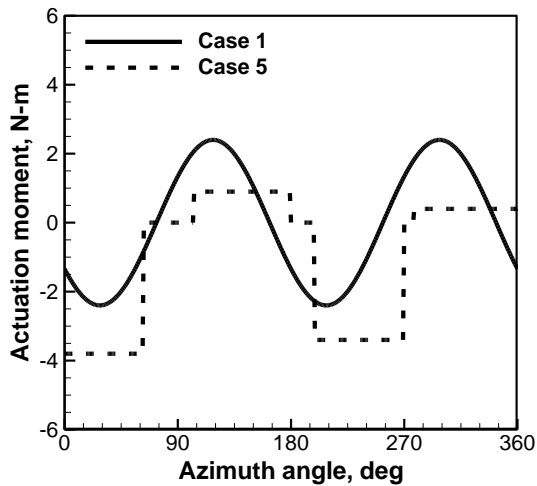


Fig. 20 Optimum input scenarios for performance improvement ($\mu = 0.34$).

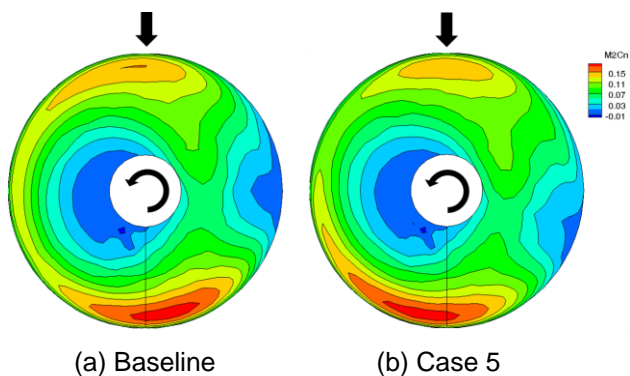


Fig. 21 Comparison of section airloads ($\mu = 0.34$).

and the overall vibration index obtained for the five different cases with respect to the baseline when the objective function is set to minimize the rotor power required only. As can be seen, the non-harmonic inputs show better power required reduction than the harmonic counterparts. The best power reduction is

observed with Case 5, which exhibits a reduction in the total power required by 1.1%, while only 0.7% power reduction is obtained in Case 1. Given the objective function set for the total power required, the vibration index becomes increased for most case. For case 2, however, the VI is decreased by about 16%. This result also assists that both rotor power and vibration reduction can be achieved if an appropriate input is adopted. In Figure 20, the best actuation schedule (Case 5) obtained for the total power reduction is compared with Case 1. A similar trend is seen between the cases but with apparent offsets. The Case 5 input produces negative twist moment when compared with Case 1. The physical mechanism leading to the improvement in the performance can be explained by airloads distribution. Figure 21 shows the section normal force coefficients obtained for ATR with Case 5 as compared with the base line uncontrolled case, presented in a contour plot. It is observed that, in the minimum power condition (Case 5), the normal force distribution becomes more uniform compared to the baseline condition. In the baseline condition, the negative lift region in the blade tip of advancing side is observed. The area of negative lift region is decreased by active twist input of the minimum power condition. More smooth distribution of airloads with Case 5 will help the reduction of the total power required. Figure 22 shows the composition of the power required for the optimum Case 5 that consists of induced power and profile power as compared to the baseline. As seen in the figure, almost all the performance improvement is caused by the induced power reduction. Because of the contribution of induced power to total power is small in high-speed forward flight condition, the effect of induced power reduction is also limited. So far, the objective function is considered with the performance perspective. The vibration response is investigated next.

Figure 23 shows the percentage reduction in the power required and the overall vibration of the five

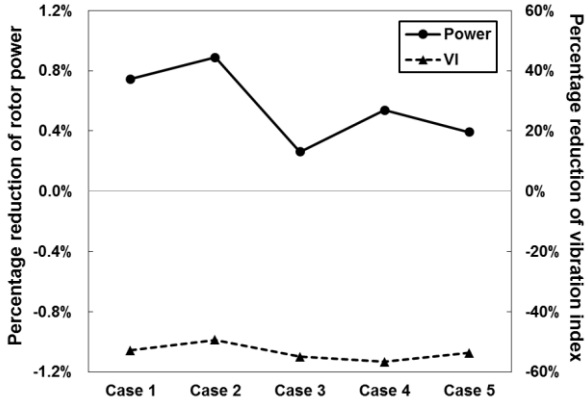


Fig. 23 Percentage reduction rotor power and vibration at the vibration optimum input ($\mu = 0.34$).

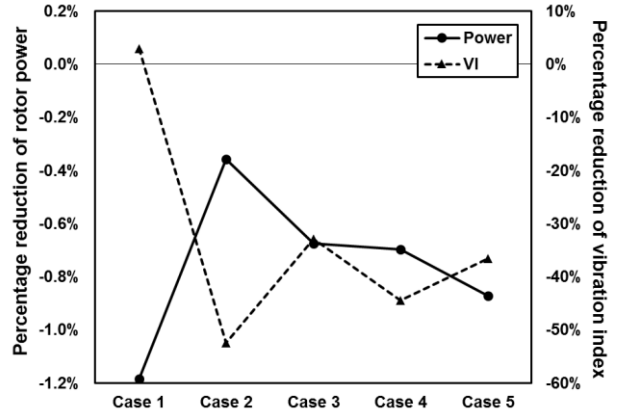


Fig. 26 Percentage reduction of rotor power and vibration at the simultaneous optimum input ($\mu = 0.34$).

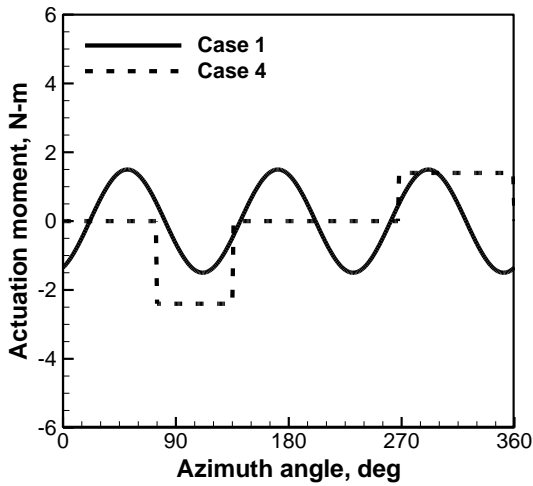


Fig. 24 Optimum input scenarios for vibration reduction ($\mu = 0.34$).

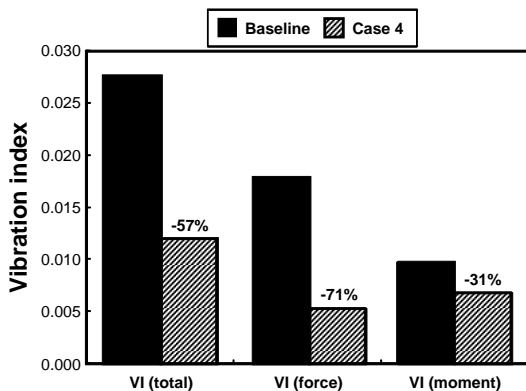


Fig. 25 Composition of vibration at the minimum vibration condition ($\mu = 0.34$).

control scenarios when the objective function is dealt with the rotor vibration only. As expected, the vibration levels for all the cases show significant reduction while the total power required indicates increase according to the active twist schedules. Among the active twist inputs, Case 4 exhibits the best vibration reduction, however, the differences of maximum vibration reduction values are small in this flight condition. The non-harmonic twist schedules show better vibration reduction gain than the harmonic counterparts, moreover the increases of the total power required are smaller than the harmonic counterparts that given the objective function set for the vibration. In Fig. 24, the best active twist schedules (Case 4) obtained for the vibration is compared with that of Case 1. The two cases show different wave forms. As can be seen, the Case 4 input needs only half of entire range. It indicates that only half actuating energy is necessary to reduce rotor vibration as compared with Case 1. Figure 25 shows the composition of the vibration index for Case 4. Both the shear force and moment components become decreased collectively leading to a reduction of about 57% based on the baseline condition. The relatively small decrease in moment components prevented the overall vibration reduction.

A simultaneous reduction of the power required and the overall vibration is attempted using the multi-objective function. Figure 26 shows the percentage reduction of power required and the overall vibration with respect to the baseline values. With the multi-objective optimization, the total power and the overall vibration are decreased simultaneously for almost cases considered. In the Case 1, the vibration increased by 3%. It can be caused by over-weighted factor at the performance parameter for the Case 1. It is indicated that the weight factors need to adjust to obtain desired optimum gains for performance or vibration.

4. CONCLUSIONS

In this work, the optimum active twist input scenario of HART II ATR is found using the optimization framework at various flight regimes. A total of five different actuation schedules are considered for the best vibration reduction and/or performance improvement. The active twist schemes include a single harmonic, multiple harmonic, and three other segmented non-harmonic actuation inputs. The following conclusions are drawn from the study.

1) The amplitude/phase sweep study reveals that the proposed optimization framework is produced reliable results for the vibration reduction and performance improvement. Additional gains such as 20% more reduction in the vibration level are obtained with the optimum algorithm.

2) The optimization results indicate that the reduction in vibration and/or power required can be achieved when suitable twist control law is applied. In general, the non-uniform actuation scenario is more suited to maximize the performance while the harmonic-based actuation shows slightly better performance in reducing the vibration.

3) The physical mechanism leading to performance gain is found illustrating the distribution of section airloads over the rotor disk. The alleviation of peak loads in the rear and the retreating region of the disk is observed to redistribute the airloads due to the actuation inputs.

4) A simultaneous vibration reduction is reached for all the test cases considered. The twist actuation with Case 4 scenario demonstrates the best vibration reduction and performance improvement in descending flight condition. About 50% vibration reduction along with 2.2% reduction in the power required is obtained.

5) For high-speed flight condition, rotor performance improved by up to 1.1% and vibration reduced by up to 57% as compared to the baseline values. For the single harmonic input, rotor performance improved by up to 0.7% and vibration reduced by up to 52% only. In particular, the non-harmonic ATR input proposed first in this paper shows great potential for performance improvement and vibration reduction.

ACKNOWLEDGEMENT

This research was supported by Basic Science Research Program through the National Research Foundation of Korea (NRF) funded by the Ministry of Education (2014R1A1A2057311).

5. REFERENCES

- [1] Chen, P., and Chopra, I., "Induced Strain Actuation of Composite Beams and Rotor Blades with Embedded Piezoceramic Elements," *Smart Materials and Structures*, Vol. 5, 1996, pp. 35-48.
- [2] Chopra, I., "Status of Application of Smart Structures Technology to Rotorcraft Systems Piezoceramic Elements," *Journal of the American Helicopter Society*, Vol. 45, No. 4, 2000, pp. 228-252.
- [3] Thakkar, D., and Ganguli, R., "Active Twist Control of Smart Helicopter Rotor – a Survey", *Journal of Aerospace Science and Technology*, Vol. 57, 2005, pp. 429-448.
- [4] Pawar, P. M., and Jung, S. N., "Single-Crystal-Material-Based Induced-Shear Actuation for Vibration Reduction of Helicopters with Composite Rotor System," *Smart Materials and Structures*, Vol. 17, 2008, pp. 1-11.
- [5] Wilbur, M. L., Yeager, W. T., and Sekula, M. K., "Further Examination of the Vibratory Loads Reduction Results from the NASA/Army/MIT Active Twist Rotor Test", *American Helicopter Society 58th Annual Forum Proceedings*, Montreal, Canada, 2002.
- [6] Fogarty, D. E., Wilbur, M. L., and Sekula, M. K., "A Computational Study of BVI Noise Reduction Using Active Twist Control", *American Helicopter Society 66th Annual Forum Proceedings*, Phoenix, AZ, 2010.
- [7] Yeo, H., "Assessment of Active Controls for Rotor Performance Enhancement," *Journal of the American Helicopter Society*, Vol. 53, No. 2, 2008, pp. 152-163.
- [8] Lim, J. W., Boyd, Jr., D. D., Hoffmann, F., van der Wall, B. G., Kim, D. H., Jung, S. N., You, Y. H., Tanabe, Y., Bailly, J., Lienard, C., and Delrieux, Y., "Aeromechanical Evaluation of Smart-Twisting Active Rotor," *Proceedings of the 40th European Rotorcraft Forum*, Southampton, U.K., 2014.
- [9] Zhang, Q., Hoffmann, F., and van der Wall, B. G., "Benefit Studies for Rotor with Active Twist Control using Weak Fluid-Structure Coupling," *Proceedings of the 35th European Rotorcraft Forum*, Hamburg, Germany, 2009.
- [10] Bailly, J., and Delrieux, Y., "Improvement of Noise Reduction and Performance for Helicopter Model Rotor Blade by Active Twist Actuation," *Proceedings of the 35th European Rotorcraft Forum*, Hamburg, Germany, 2009.
- [11] Fogarty, D. E., Wilbur, M. L., and Sekula, M. K.,

“The Effect of Non-Harmonic Active Twist Actuation on BVI Noise,” *American Helicopter Society 67th Annual Forum Proceedings*, Virginia Beach, VA, 2011.

- [12] Jain, R., Yeo, H., and Chopra, I., “Computational Fluid Dynamics- Computational Structural Dynamics Analysis of Active Control of Helicopter Rotor for Performance Improvement”, *Journal of the American Helicopter Society*, Vol. 55, No. 4, 2010.
- [13] Dhadwal, M. K., Jung, S. N., and Kim, C. J., “Advanced Particle Swarm Assisted Genetic Algorithm for Constrained Optimization Problems,” *Computational Optimization and Applications*, Vol. 58, No. 3, 2014, pp. 781-806.
- [14] Johnson, W., *CAMRAD II: Comprehensive Analytical Model of Rotorcraft Aerodynamics and Dynamics*, Johnson Aeronautics, Palo Alto, CA, 1992.
- [15] Anonymous, “Requirements for Rotorcraft Vibration Specifications, Modeling and Testing”, *Aeronautical Design Standard, Standard Practice, ADS-27A-SP*, US Army Aviation and Missile Command, Redstone Arsenal, Alabama, 2006.
- [16] van der Wall, B. G., 2nd HHC Aeroacoustic Rotor Test (HART II) – Part I: Test Documentation, *Institute Report IB 111-2003/31*, German Aerospace Center (DLR), Braunschweig, Germany, 2003.
- [17] Yeo, H., Romander, E. A., and Norman, T. R., “Investigation of Rotor Performance and Loads of a UH-60A Individual Blade Control System,” *Journal of the American Helicopter Society*, Vol. 56, No. 4, 2011, pp. 1-18.
- [18] Johnson, W., *Helicopter Theory*, Dover, 1994.
- [19] You, Y. H., Park, J. S., and Jung, S. N., “Comprehensive Code Validation on Airloads and Aeroelastic Responses of the HART II Rotor”, *International Journal of Aeronautical and Space Science*, Vol. 11, No.2, 2010, pp. 145-153.
- [20] Jung, S. N., Sa, J. H., You, Y. H., Park, J. S., and Park, S. H., "Loose Fluid-structure Coupled Approach for a Rotor in Descent Incorporating Fuselage Effects," *Journal of Aircraft*, Vol. 50, No. 4, July 2013, pp. 1016-1026.